

Symmetric and asymmetric excitations of a strong-leg quantum spin ladder

D. Schmidiger, S. Mühlbauer, and A. Zheludev*

Neutron Scattering and Magnetism, Laboratory for Solid State Physics, ETH Zürich, Switzerland

P. Bouillot

*Department of Medical Imaging and Information Sciences, Interventional Neuroradiology Unit,
University Hospitals of Geneva, Geneva 1211, Switzerland and
Laboratory for Hydraulic Machines, Ecole Polytechnique Fédérale de Lausanne, 1015 Lausanne, Switzerland*

T. Giamarchi

DPMC-MaNEP, University of Geneva, Geneva Switzerland

C. Kollath

HISKP, Universität Bonn, Nussallee 14-16, D-53115 Bonn, Germany.

G. Ehlers

Quantum Condensed Matter Division, Oak Ridge National Laboratory, Oak Ridge, Tennessee 37831, USA

A. M. Tsvelik

*Department of Condensed Matter Physics and Materials Science,
Brookhaven National Laboratory, Upton, New York 11973-5000, USA*

The zero-field excitation spectrum of the strong-leg spin ladder $(\text{C}_7\text{H}_{10}\text{N})_2\text{CuBr}_4$ is studied with a neutron time-of-flight technique. The spectrum is decomposed into its symmetric and asymmetric parts with respect to the rung momentum and compared with theoretical results obtained by the density matrix renormalization group method. Additionally, the calculated dynamical correlations are shown for a wide range of rung and leg coupling ratios in order to point out the evolution of arising excitations, as e.g. of the two-magnon bound state from the strong to the weak coupling limit.

I. INTRODUCTION

The discovery of novel materials as clean realizations of quasi-one dimensional spin Hamiltonians enabled the study of one dimensional many-body physics^{1,2} and fascinating phenomena such as Luttinger-liquid behavior³⁻⁶ or (quantum) phase transitions of gapped quantum magnets⁷⁻¹⁰, in quantitative agreement with theoretical and numerical predictions. Among these systems, the Heisenberg AF two-leg spin-ladder¹¹ belongs to the simplest models, yet featuring non-trivial physics. Recently the possibility to control such systems with the application of a magnetic field large enough to induce sizeable changes in the magnetization has allowed to explore a huge variety of novel physical phenomena¹².

Lately, a lot of effort was put in the study of dimerized *strong-rung* spin-ladders, such as e.g. the organometallic compounds $(\text{CH}_3)_2\text{CHNH}_3\text{CuCl}_3$ (IPA- CuCl_3)^{10,13,14} or $(\text{C}_5\text{H}_{12}\text{N})_2\text{CuBr}_4$ (BPCP)^{6,7,15,16}. In this coupling limit, the zero-field excitation spectrum is dominated by gapped but hardly mobile dimer triplet excitations on the rung. Nowadays, the basic underlying physics at zero magnetic field can be regarded as well established: Analytical solutions are provided by e.g. the strong-coupling approach^{17,18}, starting from non-interacting dimers.

Contrarily, the physics of *strong-leg* spin ladders remained much more elusive, mainly due to the lack of

suitable analytic approaches in particular for the regime $J_{\text{rung}}/J_{\text{leg}} \approx 1$. The existence of the spin liquid ground state and the widely dispersive gapped magnon is less obvious and originates in a subtle Haldane mechanism^{19,20}.

In contrast to the *strong-rung* limit, two-magnon excitations become progressively more important. The strong but short-ranged attractive potential between magnons leads to pronounced two-magnon bound states below a two-magnon continuum. So far, two-magnon excitations in spin-ladders were observed in the cuprate material $\text{Sr}_{14}\text{Cu}_{24}\text{O}_{41}$ ²¹ and more recently, in the organometallic low-energy scale material $(\text{C}_7\text{H}_{10}\text{N})_2\text{CuBr}_4$ (DIMPY^{22,23}). In this work, we study one- and two-magnon excitations in the latter material with a complementary technique and thereby extend the measurements of Ref. 24 and 25.

DIMPY is currently the cleanest⁴¹ realization of a *strong-leg* spin-ladder material. It crystallizes in a monoclinic structure with space group $\text{P}2(1)/n$ and lattice constants²² $a = 7.504\text{\AA}$, $b = 31.61\text{\AA}$, $c = 8.202\text{\AA}$ and $\beta = 98.98^\circ$. A depiction of the unit cell content can be found in Ref. 24. Cu^{2+} ions with an effective spin $S = 1/2$ in a tetrahedral environment of Br^- ions are interacting through Cu-Br-Br-Cu superexchange pathways, thereby building a ladder-like spin-network. DimpY features two different ladder systems, both running along the crystallographic \mathbf{a} -axis but being described by distinct rung vectors $\mathbf{d}_{1,2} = (0.423, \pm 0.256, 0.293)$, in frac-

tional coordinates²². Recent zero-field triple-axis neutron scattering experiments in combination with DMRG calculations indicated that the low-energy physics is governed by the Heisenberg spin-ladder Hamiltonian

$$\mathcal{H} = J_{\text{leg}} \sum_l \sum_{j=1}^2 \mathbf{S}_{l,j} \cdot \mathbf{S}_{l+1,j} + J_{\text{rung}} \sum_l \mathbf{S}_{l,1} \cdot \mathbf{S}_{l,2}. \quad (1)$$

Neutron experiments in combination with PCUT calculations estimated $J_{\text{leg}}/J_{\text{rung}} \approx 2.2(2)$, while careful measurements of the magnon dispersion²⁴ in combination with density matrix renormalization group (DMRG) calculations²⁵ determined the exchange constants to be $J_{\text{leg}} = 1.42(6)$ meV and $J_{\text{rung}} = 0.82(2)$ meV. Additional intra-ladder interactions were found to be insignificant²⁴ while low-temperature specific heat measurements²⁵ estimated inter-ladder interactions to be on the order of $6 \mu\text{eV}$. In the following, the theoretical calculations are performed using the time-dependent DMRG method with J_{rung} and J_{leg} as quoted above. For details on the calculations we refer to Ref. 25.

Due to the absence of e.g. diagonal interactions, the spin Hamiltonian possesses leg-permutation symmetry and the total dynamical structure factor $\mathcal{S}(\mathbf{q}, \omega)$ decomposes into a symmetric $\mathcal{S}_+(\mathbf{q}, \omega)$ and asymmetric $\mathcal{S}_-(\mathbf{q}, \omega)$ part²⁴,

$$\mathcal{S}(\mathbf{q}, \omega) = s^+(\mathbf{q}) \mathcal{S}_+(\mathbf{q}, \omega) + s^-(\mathbf{q}) \mathcal{S}_-(\mathbf{q}, \omega), \quad (2)$$

where $s^-(\mathbf{q})$ and $s^+(\mathbf{q})$ denote the asymmetric and symmetric structure factor respectively. Assuming the two ladder systems with $\mathbf{d}_{1,2}$ to be non-interacting, they are given by

$$4 s^\pm(\mathbf{q}) = 2 \pm \cos(\mathbf{q} \cdot \mathbf{d}_1) \pm \cos(\mathbf{q} \cdot \mathbf{d}_2). \quad (3)$$

Odd and even number of magnon excitations contribute to the asymmetric and symmetric channel respectively.

In neutron scattering experiments, the partial differential cross section is measured. For magnetic scattering as discussed in this work, it is given by²⁶

$$\frac{d^2\sigma}{d\Omega d\omega} \propto N \frac{k_f}{k_i} |F(\mathbf{q})|^2 \mathcal{S}(\mathbf{q}, \omega), \quad (4)$$

where N denotes the number of unit cells in the sample, $F(\mathbf{q})$ the magnetic form factor, \mathbf{k}_i (\mathbf{k}_f) the wavevector of the incident (final) neutrons and $\mathbf{q} = \mathbf{k}_f - \mathbf{k}_i$ the momentum transfer. The latter can be written as $\mathbf{q} = h\mathbf{a}^* + k\mathbf{b}^* + l\mathbf{c}^*$ with \mathbf{a}^* , \mathbf{b}^* and \mathbf{c}^* describing the reciprocal lattice vectors of the crystal. Due to the different structure factors of the symmetric and asymmetric channel, symmetric and asymmetric excitations can be fully separated in a neutron scattering experiment.

In recent experiments, the single magnon dispersion was measured by triple-axis neutron scattering and found

to be persisting throughout the complete Brillouin zone, confirming the leg-permutation symmetry²⁴. In subsequent triple-axis experiments, a two-magnon bound state was observed by performing scans at three positions in reciprocal space, $(h, k, l) = (\eta, 0, -1.44 \cdot \eta)$ with $\eta = 0.5, 0.625$ and 0.75 , quantitatively confirming numerical density matrix renormalization group (DMRG) calculation of $\mathcal{S}_+(\mathbf{q}, \omega)$ ²⁵.

The goal of this work is twofold: First, we extend the measurements of Ref. 24 and 25 by using the complementary neutron time-of-flight technique, since a detailed analysis of the symmetric and asymmetric zero-field spectrum of DIMPY has not yet been performed. We study the bound state in detail, definitely prove the leg-permutation symmetry and separate the symmetry channels completely. Secondly, DMRG calculations of the dynamical structure factor were performed for different coupling ratios $0.5 < J_{\text{leg}}/J_{\text{rung}} < \infty$. This enables us to numerically observe the evolution of excitations from the strong-rung to the strong-leg regime and to compare it to existing analytic results.

II. EXPERIMENT

For the present experiment, the same sample as in Ref. 24,25 was used. It consisted of four fully deuterated single crystals $(\text{C}_7\text{D}_{10}\text{N})_2\text{CuBr}_4$ with a total mass of 3.7 g and co-aligned to a mosaic spread better than 1.5° . Measurements were performed at the CNCS cold neutron chopper spectrometer²⁷ at SNS spallation source. Temperature was controlled with a conventional ^4He -cryostat and the sample was mounted with the \mathbf{b} -axis vertical. Measurements were performed at $T = 1.5$ K and background data was collected at 50 K and 110 K. The incident energy was fixed to 4.2 meV and the sample was rotated by 180° in steps of 5° . Intensity was normalized to the proton charge on the target: $1.5 \mu\text{C}$ (40 minutes counting time) per rotation step for the 1.5 K and $0.75 \mu\text{C}$ for the 50 K and 110 K measurement respectively.

III. RESULTS AND DISCUSSION

A. Integrated intensity and structure factor

Due to the exceptional one-dimensional nature of DIMPY, no dispersion along the perpendicular directions \mathbf{b}^* and \mathbf{c}^* was observed previously²⁸. Neutron time-of-flight data can hence be integrated along these directions, thereby improving statistics. Raw data at $T = 1.5$ K and 50 K, integrated along \mathbf{b}^* and \mathbf{c}^* using the Horace program²⁹ is shown in figure 1a,b.

At 1.5 K both the single-magnon excitation and the two-magnon bound state are observed over four Brillouin zones. However, the magnetic signal is contaminated by T -dependent and T -independent contributions. The T -dependent contributions are mainly due to the inelastic

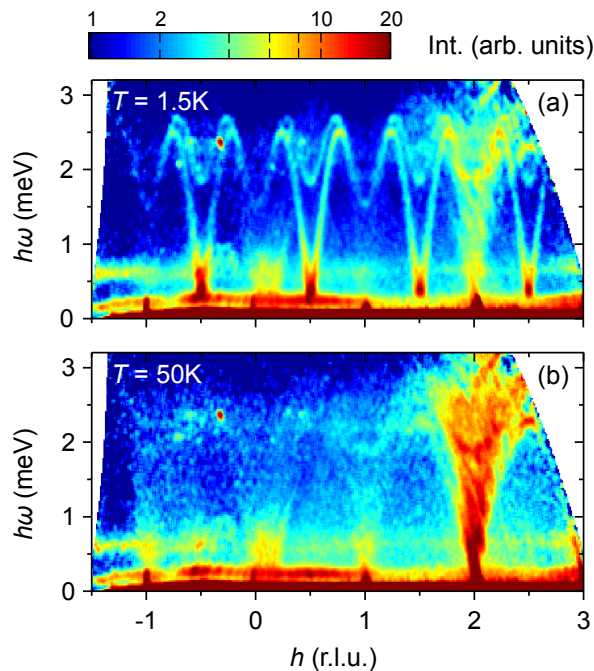


FIG. 1: (Color online) Raw data from neutron time-of-flight experiments in $(\text{C}_7\text{D}_{10}\text{N})_2\text{CuBr}_4$, measured at (a) $T = 1.5$ K and (b) $T = 50$ K. Data was integrated along the non-dispersive \mathbf{b}^* and \mathbf{c}^* direction. Intensity is shown as a function of energy transfer $\hbar\omega$ and momentum transfer along the leg h , in reciprocal lattice units.

phonon scattering. This is in contrast to T independent background, which can stem from both coherent and incoherent scattering by the sample and equipment. Such contributions are evident in comparison with the measurement at 50 K (fig. 1b).

Background subtraction was performed taking both of these contributions into account as described in Appendix A, using the integrated data sets. In figure 2, background subtracted data is shown in the Brillouin zone $0 < h < 1$. Clearly, most of the background features are removed by our procedure.

Due to the integration process, the cosine functions in equation (3) average to zero and an equal combination of $\mathcal{S}_+(h, \omega)$ and $\mathcal{S}_-(h, \omega)$ is observed. The measured magnon dispersion agrees with the recently performed triple-axis experiment at $T = 50$ mK (black points, from Ref. 24). Moreover, the two-magnon bound state clearly persists in the region $0.2 < h < 0.8$ and is consistent with the three constant- \mathbf{q} scans performed in Ref. 25 (white points), while two-magnon continuum excitations are too weak to be observed under experimental conditions. The numerical calculation of $\mathcal{S}_+(h, \omega) + \mathcal{S}_-(h, \omega)$ convoluted with an approximate experimental resolution (Fig. 2b) is in quantitative agreement with the experiment, both in terms of dispersion and intensity of the two sharp modes.

In order to map out the structure factors $s^\pm(\mathbf{q})$, raw data at 1.5 K, 50 K and 110 K was integrated around

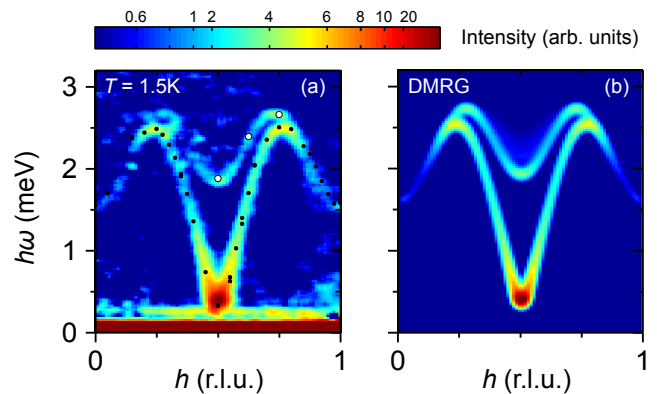


FIG. 2: (Color online) (a) Background subtracted data from neutron time-of-flight experiments in $(\text{C}_7\text{D}_{10}\text{N})_2\text{CuBr}_4$, integrated along the \mathbf{b}^* and \mathbf{c}^* direction. Intensity is shown as a function of energy transfer $\hbar\omega$ and momentum transfer along the leg. Black and white points correspond to triple-axis measurements of the magnon and two-magnon bound state excitations (Ref. 24,25). (b) Numerical DMRG calculation of the dynamical structure factor $\mathcal{S}_+(h, \omega) + \mathcal{S}_-(h, \omega)$, convoluted with experimental resolution. The measured and calculated spectra show remarkable agreement.

the magnetic zone center $h = [0.45, 0.55]$ rlu and in the energy range $\hbar\omega = [0.2, 0.6]$ meV and $[1.75, 2.05]$ meV, enclosing the magnon and two-magnon bound states, respectively. As described in Appendix A, the instrumental and phonon background were separated, extrapolated to 1.5 K and subtracted (fig. 3a,c).

The structure factors $s_h^\pm(k, l)$ given by equation (3) were calculated for $h = 0.5$ on the same k, l -grid as experimental data (fig. 3 b,d). They were multiplied by the magnetic form factor of the Cu^{2+} ion, given by $|F_h(k, l)|^2 \approx |\langle j_0 \rangle_h(k, l)|^2$ and with the function j_0 as numerically calculated in Ref. 30.

The cut around the single magnon excitation (fig. 3a) clearly follows the predicted asymmetric channel structure factor $s_h^-(k, l)$ (fig. 3b). Although the vertical coverage of a 2D time-of-flight detector is limited by $\pm 16^\circ$, the exceptionally long \mathbf{b} -axis of DIMPY ($b = 31.61$ Å) enables to observe a full period of the structure factor in vertical direction.

Although the signal for the cut around the two-magnon bound state (fig. 3c) is much weaker, we observe enhanced intensity in the range $-2 < l < 0$ with $-1 < k < 1$ while it is basically zero for $0 < l < 2$. This is in agreement with the calculated variation of the symmetric structure factor $s_h^+(k, l)$ as shown in fig. 3d. The assumption of two non-interacting ladder systems with structure factors as in equation (3) is hence found to be valid.

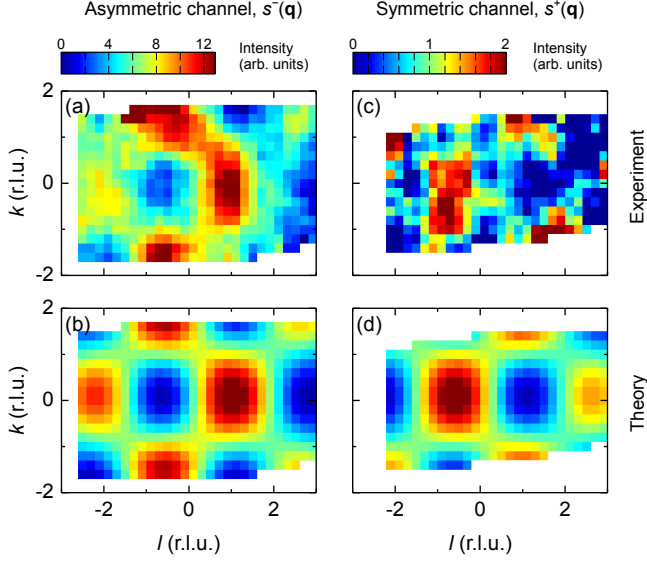


FIG. 3: (Color online) Background subtracted data $\mathcal{I}_{h,\omega}^{\text{sub}}(k, l)$, as a function of momentum transfer along the perpendicular directions \mathbf{b}^* and \mathbf{c}^* , in order to visualize (a) the asymmetric and (b) the symmetric structure factors $s_{\hbar}^{\pm}(k, l)$. Data was integrated along $h = [0.45, 0.55]$ rlu and in the energy range (a) $\hbar\omega = [0.2, 0.6]$ meV and (c) $[1.75, 2.05]$ meV. The corresponding calculation of the asymmetric and symmetric structure factor $s_{\hbar}^{\pm}(k, l)$ weighted by the magnetic form factor are shown in (b) and (d).

B. Channel Separation

As a next step, the two symmetry channels were separated. The basic idea was to divide the 4D data set of 2D cuts by integrating along small ranges in h and $\hbar\omega$ and to determine the contribution of the asymmetric and symmetric channel for each value of h_i and $\hbar\omega_i$, assuming that the structure factors are given by equation (3).

The h - $\hbar\omega$ -plane was divided into 1600 boxes $(h_i, \hbar\omega_i)$ of the size $0.025 \text{ rlu} \times 0.075 \text{ meV}$. For each box $(h_i, \hbar\omega_i)$, data measured at 1.5K, 50K and 110K was integrated along a small range $h_i \pm 0.025 \text{ rlu}$ and $\hbar\omega_i \pm 0.075 \text{ meV}$, leaving 2D data sets $\mathcal{I}_{h_i, \omega_i}^T(k, l)$. Background subtraction was performed for each $(h_i, \hbar\omega_i)$ using the data sets $\mathcal{I}_{h_i, \omega_i}^T(k, l)$ with $T = 1.5 \text{ K}, 50 \text{ K}$ and 110 K , as described in Appendix A.

The structure factor for the asymmetric and symmetric channel $s_{\hbar}^{\pm}(k, l)$ were calculated on the same grid as the data. Two masks $M_{h_i, \omega_i}^{\pm}(k, l)$ were defined by

$$M_{h_i, \omega_i}^{\pm}(k, l) = \begin{cases} s_{\hbar}^{\pm}(k, l)^{-1} |F_{h_i}(k, l)|^{-2} & s_{\hbar}^{\pm}(k, l) \geq L_{\pm} \\ 0 & \text{else} \end{cases} \quad (5)$$

such that the asymmetric and symmetric masks $M_{h_i, \omega_i}^{\pm}(k, l)$ cut out data in the region where intensity from the corresponding channel is expected by the struc-

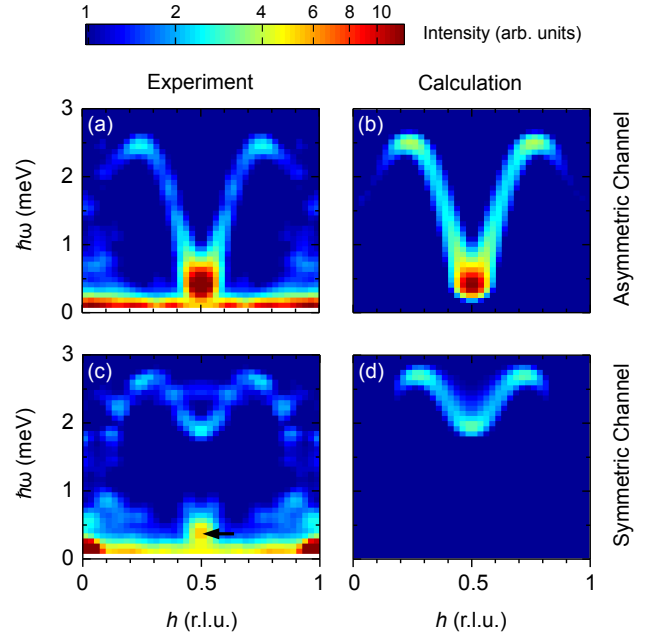


FIG. 4: (Color online) Separation of the asymmetric and symmetric channel in $(\text{C}_7\text{D}_{10}\text{N})_2\text{CuBr}_4$. (a) asymmetric and (c) symmetric contribution extracted from raw data as explained in the text. A spurious remainder of the single-magnon excitation is still visible in the separated symmetric contribution (c) (black arrow). DMRG calculation of (b) $\mathcal{S}_-(h, \omega)$ and (d) $\mathcal{S}_+(h, \omega)$, convoluted with a similar resolution as in (a).

ture factor. The threshold for the channel were taken to be $L_+ = 0.8$ and $L_- = 0.85$, respectively⁴².

In order to determine the asymmetric contribution, background subtracted data $\mathcal{I}_{h_i, \omega_i}^{\text{sub}}(k, l)$ was multiplied elementwise by the asymmetric mask $M_{h_i, \omega_i}^-(k, l)$, summed up and divided by the number of non-zero elements - leaving one number $I^-(h_i, \omega_i)$ describing the asymmetric contribution at the position (h_i, ω_i) . The same procedure was performed for the symmetric mask $M_{h_i, \omega_i}^+(k, l)$ leading to the symmetric contribution $I^+(h_i, \omega_i)$ at (h_i, ω_i) .

The separated and symmetrized contributions $I^-(h, \omega)$ and $I^+(h, \omega)$ in the first Brillouin zone $0 < h < 1$ are shown in figure 4a,c respectively. $I^-(h, \omega)$ clearly contains the single-magnon excitation while no contribution from the two-magnon bound state is visible. Figure 4 shows the DMRG calculation of $\mathcal{S}_-(h, \omega)$, convoluted with a similar resolution as in fig. 4a. However, due to the separation process, the intensity cannot be compared anymore. The two-magnon bound state is clearly visible in the separated even channel $I^+(h, \omega)$, in agreement with the calculated $\mathcal{S}_+(h, \omega)$ (fig. 4d). $I^+(h, \omega)$ still contains a 'ghost' of the single-magnon excitation (black arrow) an artefact of the separation process.

IV. DISCUSSION

The results can be summarized as follows. (1) The excitations spectrum of DIMPY is dominated by the well-known magnon excitation as well as a strong and highly dispersive two-magnon bound state, persisting throughout about 60% of the Brillouin zone. The intensity and dispersion of both modes are in full agreement with the DMRG calculations. (2) The symmetric and asymmetric structure factor follows the prediction for non-interacting ladder systems with rung vectors $d_{1,2}$ and can directly be mapped out in a TOF experiment. (3) DIMPY features the leg-permutation symmetry. The asymmetric and symmetric excitation channel can be fully separated. The former contains the magnon excitation while the latter contains the two-magnon bound state.

In order to put results into context, we show in the following DMRG calculations of the momentum- and frequency resolved dynamical structure factor in both symmetry channels from the strong-rung to the strong-leg regime. This enables us to relate to numerous aspects of the spin-ladder problem in either coupling regimes which were studied in detail before, both analytically and numerically^{20,31–37}.

The calculations were performed for different coupling ratios $x = J_{\text{leg}}/J_{\text{rung}}$, particularly for $x = 0.5, 1, 1.72, 5, 10$, with J_{leg} fixed to unity, as well as for the spin chain ($x \rightarrow \infty$). Figure 5 shows the calculated structure factor in the asymmetric (*left*) and symmetric (*right*) channel for different coupling ratios. It is shown as a function of energy $\hbar\omega$ and momentum along the leg of the ladder, $q_{\parallel} := \mathbf{q} \cdot \mathbf{a}$.

In the strong-rung regime with $x < 1$ (fig. 5a,b), the spin ladder consists of weakly interacting dimers. The asymmetric dynamical structure factor is dominated by a hardly dispersive magnon excitation with a gap $\Delta \simeq J_{\text{rung}} - J_{\text{leg}}$ and a bandwidth $W \simeq 2J_{\text{leg}}$. The symmetric channel contains a weak two-magnon continuum as well as a $S = 1$ bound state existing in a narrow region around the magnetic zone center $q_{\parallel} = \pi$.

For strong-rung ladders, the dispersion³⁵ and the spectral weight of the magnon, the two-magnon continuum as well as the bound states were calculated using the strong-coupling expansion^{31,33,36} and with the linked cluster series expansion³⁴. White lines in figure 5a correspond to the calculation in Ref. 34,35 and agree for $x = 0.5$. Moreover, the results indicate that for $x \rightarrow 0$, the triplet bound state exists only in a narrow q -range with $2\pi/3 < q_{\parallel} < 4\pi/3$ (i.e. in $1/3$ of the Brillouin zone) and that the spectral weight of the triplet state scales with x^2 (Ref. 31). In strong-rung ladders, two-magnon excitations are hence usually too weak to be observable by neutron scattering methods.

In contrast, for the strong-leg coupling regime $x > 1$ both the symmetric and asymmetric dynamical structure factors converge towards the two-spinon continuum excitation spectrum of the Heisenberg $S = 1/2$ spin chain for $x \rightarrow \infty$ (fig. 5f). The latter is gapless, fea-

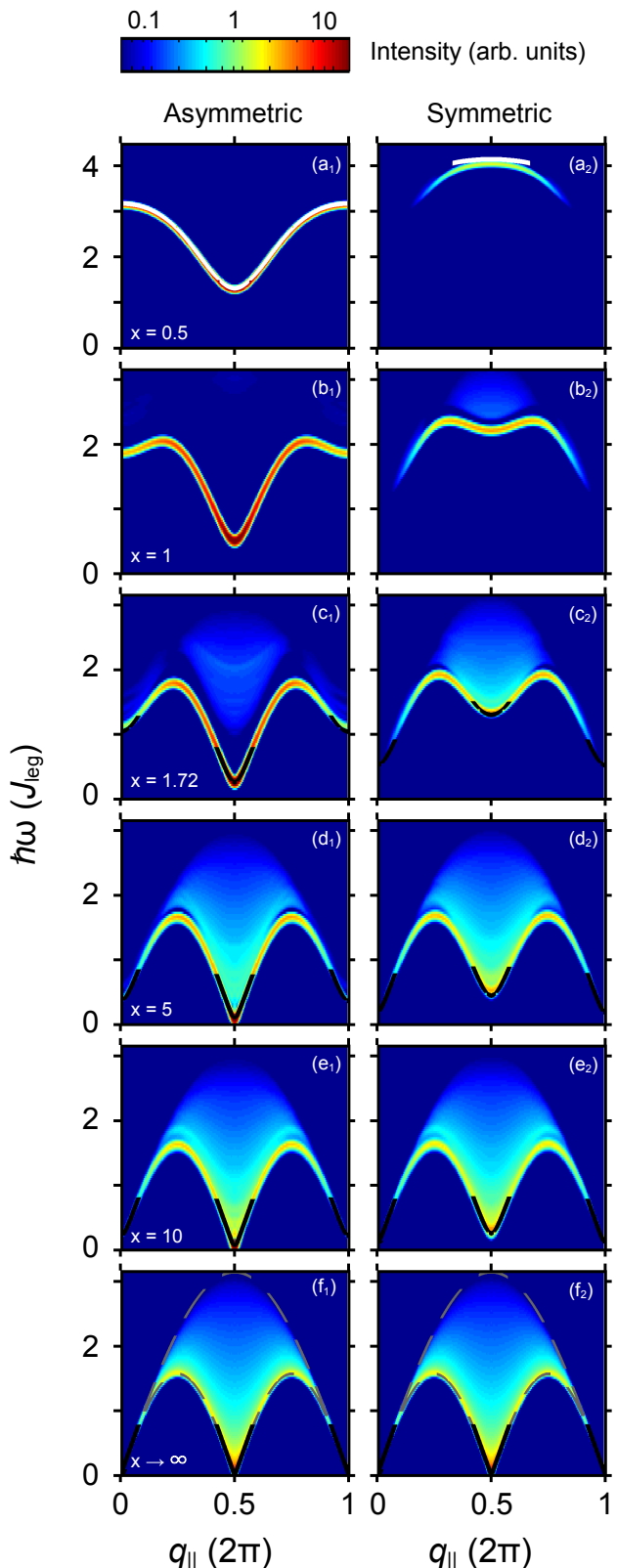


FIG. 5: (Color online) DMRG calculation of the momentum- and frequency resolved dynamic structure factor in the asymmetric (left) and symmetric (right) channel with rung momentum $q_{\perp} = \pi$ and 0 , respectively. White lines correspond to predictions from Ref. 34,35. Black lines indicate the boundaries of multi-particle continua as described in the text.

tures a bandwidth of $W = \pi J_{\text{leg}}$ and is bounded³⁹ by $\epsilon_1 = \pi J_{\text{leg}}/2 |\sin(q_{\parallel})|$ and $\epsilon_u = \pi J_{\text{leg}} |\sin(q_{\parallel}/2)|$ (grey broken lines in fig. 5f).

At finite inter-chain interaction J_{rung} , spinons are confined and asymmetric excitations acquire a spin gap of $\Delta \simeq 0.41 J_{\text{rung}}$ if $x \gg 1$ (Ref. 32). As pointed out by Shelton et al.³⁸, the bosonized Hamiltonian can be mapped onto a system of weakly interacting massive triplet and singlet Majorana fermions, with masses $m_s \simeq 3m_t$ and with the velocity of the Heisenberg spin chain, $v = \pi J_{\text{leg}}/2$. The triplet Majorana fermion is asymmetric under leg permutation symmetry (its rung momentum is $q_{\perp} = \pi$) while the singlet Majorana fermion is symmetric with $q_{\perp} = 0$. The dynamic structure factor contains various sharp and continuous single and multi Majorana fermion excitations, summarized in table I.

Excitation	q_{\perp}	$q_{\parallel, \text{min}}$	Threshold m_{thresh}
1T	π	π	$1m$
2T	0	0	$2m$
3T	π	π	$3m$
1T + 1S	π	0	$4m$
2T + 1S	0	π	$5m$

TABLE I: Multi triplet (T) and singlet (S) low energy excitations. The rung q_{\perp} denotes the symmetry channel in which these excitations appear while $q_{\parallel, \text{min}}$ determines whether they occur around π or 0. m_{thresh} describes to the gap of the corresponding excitation.

The triplet excitation (the ‘‘magnon’’) is a sharp mode around $q_{\parallel} = \pi$ only and its dispersion is described by

$$\epsilon_t = \sqrt{m^2 + v^2(q_{\parallel} - \pi)^2} \quad (6)$$

with $m \approx 0.41 J_{\text{rung}}$. The lower boundaries of the multi-particle continua are given by

$$\epsilon_1 = \sqrt{m_{\text{thresh}}^2 + v^2(q_{\parallel} - q_{\parallel, \text{min}})^2} \quad (7)$$

and can be observed either in the symmetric ($q_{\perp} = 0$) or asymmetric ($q_{\perp} = \pi$) channel. These predictions are shown as black full lines in figure 5c-f and successfully describe the lower boundary of the dynamical structure factor in the strong-leg regime, confirming the analytical predictions. In particular in the symmetric channel, the continuum around $q_{\parallel} = \pi$ corresponds to two triplet and one singlet excitation, whereas the continuum around $q_{\parallel} = 0$ results from two triplet excitations.

For the experimental value $x \approx 1.72$ in DIMPY instead of the threshold singularity the symmetric channel displays a rather well defined coherent mode. In the framework of Ref. 38 this corresponds to the three-particle bound state of two triplet and one singlet excitation. This value of x is too small for the above theory to yield good quantitative predictions, though it contains a provision for such bound state. This provision comes in the

form of the interaction the Majorana fermions originating from the coupling of uniform magnetizations of the two chains³⁸. The massive Majorana fermions interact and with the proper sign of interaction can create bound states. Nevertheless, in contrast to strong-rung spin ladders, this bound state is only 8 times weaker than the single magnon excitation at $q_{\parallel} = \pi$. Moreover, the two-magnon bound state seems not confined to a narrow q -range but persists throughout about 60% of the Brillouin zone and shows itself a structured dispersion. The latter does not yet follow the expansion based on the strong-coupling approach in Ref. 34.

Being in an intermediate coupling limit with neither $x \ll 1$ nor $x \gg 1$, the observed bound state around $q_{\parallel} = \pi$ in DIMPY can hence be understood *qualitatively* either as a bound state of two dimer-triplet excitations or a bound state of two-triplet and one singlet Majorana Fermion excitations in the language of Ref. 38, although analytic solutions from both coupling limits can not describe the bound-state *quantitatively* anymore.

V. CONCLUSION

In conclusion, detailed follow-up zero-field measurements on the strong-leg spin ladder material DIMPY were performed by the neutron time-of-flight technique. The two-magnon bound state recently observed by the triple-axis scattering technique was studied in detail and shown to be persisting throughout 60% of the Brillouin zone. The structure factor of the even and odd excitation channel was measured and shown to be consistent with the model of two non-interacting ladder systems described by the rung vectors $\mathbf{d}_{1,2}$. It was shown how the large 4D data set collected in a time-of-flight experiment can be used in a smart way in order to separate the two channels. Moreover, the evolution of the dynamical structure factor in the strong-leg regime was studied and it was shown how both the symmetric and asymmetric channel converge towards the two-spinon continuum of a spin-chain.

Acknowledgments

This work is partially supported by the Swiss National Fund under division II and through Project 6 of MANEP. Research at Oak Ridge National Laboratory’s Spallation Neutron Source was supported by the Scientific User Facilities Division, Office of Basic Energy Sciences, U. S. Department of Energy. We thank Dr. Andrey Podlesnyak and the SNS sample environment team for their support during the experiment.

A. Appendix A: Background subtraction

In the following Appendix, we briefly describe the background subtraction procedure. It is a standard approach and was performed in a similar way in e.g. Refs. 3, 40. For the present experiment, two sources of background were assumed: (1) Temperature-independent background both from the cryostat and other equipment as well as coherent and incoherent scattering from the sample²⁶ and (2) inelastic phonon scattering from the sample, proportional to the bose-factor $n(\omega) + 1$. The total signal $\mathcal{I}(\mathbf{Q}, \omega, T)$ at $T_1 = 50$ K and $T_2 = 110$ K was modelled as

$$\mathcal{I}(\mathbf{Q}, \omega, T) = \mathcal{A}(\mathbf{Q}, \omega) + \mathcal{B}(\mathbf{Q}, \omega)(n(\omega, T) + 1) \quad (8)$$

with $n(\omega) = (e^{\hbar\omega/k_B T} - 1)^{-1}$ and \mathcal{A} , \mathcal{B} describing the T-independent and T-dependent background, respectively. The background contributions can be calculated by

$$\mathcal{B}(\mathbf{Q}, \omega) = \frac{\mathcal{I}_1(\mathbf{Q}, \omega) - \mathcal{I}_2(\mathbf{Q}, \omega)}{n(\omega, T_1) - n(\omega, T_2)} \quad (9)$$

$$\mathcal{A}(\mathbf{Q}, \omega) = \mathcal{I}_1(\mathbf{Q}, \omega) - \mathcal{B}(\mathbf{Q}, \omega)(n(\omega, T_1) + 1). \quad (10)$$

The background subtracted signal at base temperature $T_0 = 1.5$ K is therefore

$$\mathcal{I}^{\text{sub}}(\mathbf{Q}, \omega) = \mathcal{I}_0(\mathbf{Q}, \omega) - \mathcal{A}(\mathbf{Q}, \omega) - \mathcal{B}(\mathbf{Q}, \omega)(n(\omega, T_0) + 1). \quad (11)$$

-
- * Electronic address: zhelud@ethz.ch; URL: <http://www.neutron.ethz.ch/>
- ¹ T. Giamarchi, Quantum physics in One Dimension (Oxford university press, 2003).
 - ² A. M. Tsvelik, Quantum Field Theory in Condensed Matter Physics (Cambridge University Press, 2007), 2nd ed.
 - ³ D. C. Dender, D. Davidović, D. H. Reich, C. Broholm, K. Lefmann and G. Aeppli, Phys. Rev. B **53**, 2583 (1996).
 - ⁴ M. B. Stone, D. H. Reich, C. Broholm, K. Lefmann, C. Rischel, C. P. Landee and M. M. Turnbull, Phys. Rev. Lett. **91**, 037205 (2003).
 - ⁵ B. Lake, D. A. Tennant, C. D. Frost and S. E. Nagler, Nature materials **4**, 329 (2005).
 - ⁶ M. Klanjšek, H. Mayaffre, C. Berthier, M. Horvatić, B. Chiari, O. Piovesana, P. Bouillot, C. Kollath, E. Orignac, R. Citro and T. Giamarchi, Phys. Rev. Lett. **101**, 137207 (2008).
 - ⁷ B. Thielemann, C. Rüegg, K. Kiefer, H. M. Rønnow, B. Normand, P. Bouillot, C. Kollath, E. Orignac, R. Citro, T. Giamarchi, et al., Phys. Rev. B **79**, 020408 (2009).
 - ⁸ B. Thielemann, C. Rüegg, H. M. Rønnow, A. M. Läuchli, J.-S. Caux, B. Normand, D. Biner, K. W. Krämer, H.-U. Güdel, J. Stahn, et al., Phys. Rev. Lett. **102**, 107204 (2009).
 - ⁹ V. S. Zapf, D. Zocco, B. R. Hansen, M. Jaime, N. Harrison, C. D. Batista, M. Kenzelmann, C. Niedermayer, A. Lacerda and A. Paduan-Filho, Phys. Rev. Lett. **96**, 077204 (2006).
 - ¹⁰ A. Zheludev, V. O. Garlea, T. Masuda, H. Manaka, L.-P. Regnault, E. Ressouche, B. Grenier, J.-H. Chung, Y. Qiu, K. Habicht, et al., Phys. Rev. B **76**, 054450 (2007).
 - ¹¹ T. Barnes, E. Dagotto, J. Riera and E. S. Swanson, Phys. Rev. B **47**, 3196 (1993).
 - ¹² T. Giamarchi, C. Rüegg and O. Tchernyshyov, Nature Physics **4**, 198 (2008).
 - ¹³ T. Masuda, A. Zheludev, H. Manaka, L.-P. Regnault, J.-H. Chung and Y. Qiu, Phys. Rev. Lett. **96**, 047210 (2006).
 - ¹⁴ T. Fischer, S. Duffe and G. S. Uhrig, EPL (Europhysics Letters) **96**, 47001 (2011).
 - ¹⁵ C. Rüegg, K. Kiefer, B. Thielemann, D. F. McMorrow, V. Zapf, B. Normand, M. B. Zvonarev, P. Bouillot, C. Kollath, T. Giamarchi, et al., Phys. Rev. Lett. **101**, 247202 (2008).
 - ¹⁶ P. Bouillot, C. Kollath, A. M. Läuchli, M. Zvonarev, B. Thielemann, C. Rüegg, E. Orignac, R. Citro, M. Klanjšek, C. Berthier, et al., Phys. Rev. B **83**, 054407 (2011).
 - ¹⁷ S. Sachdev and R. N. Bhatt, Phys. Rev. B **41**, 9323 (1990).
 - ¹⁸ S. Gopalan, T. M. Rice and M. Sigrist, Phys. Rev. B **49**, 8901 (1994).
 - ¹⁹ F. D. M. Haldane, Phys. Rev. Lett. **50**, 1153 (1983).
 - ²⁰ E. Dagotto and T. M. Rice, Science **271**, 618 (1996).
 - ²¹ S. Notbohm, P. Ribeiro, B. Lake, D. A. Tennant, K. P. Schmidt, G. S. Uhrig, C. Hess, R. Klingeler, G. Behr, B. Büchner, et al., Phys. Rev. Lett. **98**, 027403 (2007).
 - ²² A. Shapiro, C. P. Landee, M. M. Turnbull, J. Jorner, M. Deumal, J. J. Novoa, M. A. Robb and W. Lewis, Journal of the American Chemical Society **129**, 952 (2007).
 - ²³ J. Jorner-Somoza, M. Deumal, M. M. Turnbull and J. J. Novoa, Polyhedron **28**, 1965 (2009).
 - ²⁴ D. Schmidiger, S. Mühlbauer, S. N. Gvasaliya, T. Yankova and A. Zheludev, Phys. Rev. B **84**, 144421 (2011).
 - ²⁵ D. Schmidiger, P. Bouillot, S. Mühlbauer, S. Gvasaliya, C. Kollath, T. Giamarchi and A. Zheludev, Phys. Rev. Lett. **108**, 167201 (2012).
 - ²⁶ G. L. Squires, Introduction to the theory of neutron scattering (Cambridge University Press, 1978).
 - ²⁷ G. Ehlers, A. A. Podlesnyak, J. L. Niedziela, E. B. Iverson and P. E. Sokol, Review of Scientific Instruments **82**, 085108 (pages 6) (2011).
 - ²⁸ T. Hong, Y. H. Kim, C. Hotta, Y. Takano, G. Tremelling, M. M. Turnbull, C. P. Landee, H.-J. Kang, N. B. Christensen, K. Lefmann, et al., Phys. Rev. Lett. **105**, 137207 (2010).
 - ²⁹ T. G. Perring, R. A. Ewings and J. V. Duijn, unpublished.
 - ³⁰ P. J. Brown, in International Tables for Crystallography vol. C, chapter 4.4.5., edited by A. J. C. Wilson (2006).
 - ³¹ K. Damle and S. Sachdev, Phys. Rev. B **57**, 8307 (1998).
 - ³² M. Greven, R. J. Birgeneau and U. J. Wiese, Phys. Rev. Lett. **77**, 1865 (1996).
 - ³³ O. P. Sushkov and V. N. Kotov, Phys. Rev. Lett. **81**, 1941 (1998).
 - ³⁴ W. Zheng, C. J. Hamer, R. R. P. Singh, S. Trebst and H. Monien, Phys. Rev. B **63**, 144410 (2001).

- ³⁵ M. Reigrotzki, H. Tsunetsugu and T. M. Rice, *Journal of Physics: Condensed Matter* **6**, 9235 (1994).
- ³⁶ J. Oitmaa, R. R. P. Singh and W. Zheng, *Phys. Rev. B* **54**, 1009 (1996).
- ³⁷ C. Knetter, K. P. Schmidt, M. Grüniger and G. S. Uhrig, *Phys. Rev. Lett.* **87**, 167204 (2001).
- ³⁸ D. G. Shelton, A. A. Nersesyan and A. M. Tsvelik, *Phys. Rev. B* **53**, 8521 (1996).
- ³⁹ G. Müller, H. Thomas, H. Beck and J. C. Bonner, *Phys. Rev. B* **24**, 1429 (1981).
- ⁴⁰ M. B. Stone, I. A. Zaliznyak, T. Hong, C. L. Broholm and D. H. Reich, *Nature* **440**, 187 (2006).
- ⁴¹ The inter-ladder interaction was found to be $J' \approx 6 \mu\text{eV}$, more than 2 orders of magnitude smaller than J_{leg} and J_{rung} .
- ⁴² The threshold for the symmetric channel was taken to be slightly lower in order to resolve the two-magnon bound state which is much weaker than the magnon excitations.